

High-Resolution Analysis of Chromosomal Breakpoints and Genomic Instability Identifies *PTPRD* as a Candidate Tumor Suppressor Gene in Neuroblastoma

Raymond L. Stallings,¹ Prakash Nair,¹ John M. Maris,² Daniel Catchpoole,³ Michael McDermott,⁴ Anne O'Meara,⁵ and Fin Breatnach⁵

¹Children's Cancer Research Institute and Department of Pediatrics, University of Texas Health Science Center at San Antonio, San Antonio, Texas; ²Division of Oncology, Children's Hospital of Philadelphia and Department of Pediatrics, University of Pennsylvania School of Medicine, Philadelphia, Pennsylvania; ³The Tumor Bank, Children's Hospital at Westmead, Sydney, New South Wales, Australia; and Departments of ⁴Pathology and ⁵Oncology, Our Lady's Hospital for Sick Children, Dublin, Ireland

Abstract

Although neuroblastoma is characterized by numerous recurrent, large-scale chromosomal imbalances, the genes targeted by such imbalances have remained elusive. We have applied whole-genome oligonucleotide array comparative genomic hybridization (median probe spacing 6 kb) to 56 neuroblastoma tumors and cell lines to identify genes involved with disease pathogenesis. This set of tumors was selected for having either 11q loss or *MYCN* amplification, abnormalities that define the two most common genetic subtypes of metastatic neuroblastoma. Our analyses have permitted us to map large-scale chromosomal imbalances and high-level amplifications at exon-level resolution and to identify novel microdeletions and duplications. Chromosomal breakpoints ($n = 467$) generating imbalances >2 Mb were mapped to intervals ranging between 6 and 50 kb in size, providing substantial information on each abnormality. For example, breakpoints leading to large-scale hemizygous loss of chromosome 11q were highly clustered and preferentially associated with segmental duplications. High-level amplifications of *MYCN* were extremely complex, often resulting in a series of discontinuous regions of amplification. Imbalances ($n = 540$) <2 Mb long were also detected. Although the majority (78%) of these imbalances mapped to segmentally duplicated regions and primarily reflect constitutional copy number polymorphisms, many subtle imbalances were detected that are likely somatically acquired alterations and include genes involved with tumorigenesis, apoptosis, or neural cell differentiation. The most frequent microdeletion involved the *PTPRD* locus, indicating a possible tumor suppressor function for this gene. (Cancer Res 2006; 66(7): 3673-80)

Introduction

Neuroblastomas are derived from primitive cells of the sympathetic nervous system and account for ~15% of all childhood cancer deaths (see ref. 1 for review). These tumors are particularly noted for extensive heterogeneity in clinical behavior, ranging from spontaneous regression to aggressive clinical course

and death from disease. Patient age, tumor stage, and several different genetic abnormalities are important factors that influence clinical outcome. Loss of 1p and 11q, gain of 17q, and amplification of the *MYCN* oncogene are particularly strong genetic indicators of poor disease outcome (2–5). Two of these abnormalities, loss of 11q and *MYCN* amplification, form the basis for dividing advanced-stage neuroblastomas into genetic subtypes due to their rather striking inverse distribution in tumors (6, 7). Many other recurrent partial chromosomal imbalances, including loss of 3p, 4p, 9p, and 14q and gain of 1q, 2p, 7q, and 11p, have been identified by metaphase comparative genomic hybridization (CGH) or allotyping studies (5–7). Although many of these chromosomal imbalances undoubtedly play major roles in neuroblastoma pathogenesis, the targeted genes and genetic pathways have remained elusive.

Higher-resolution array CGH analyses hold great promise for identifying neuroblastoma tumor suppressor and oncogenes by narrowing down the critical regions that harbor the genes. CGH analysis of neuroblastoma using either BAC (8) or cDNA (9) microarrays have been used to detect more subtle chromosomal imbalances and to narrow the intervals containing genes important for neuroblastoma pathogenesis. Mosse et al. (8) used arrays containing ~4,100 BAC clones (~1-Mb average spacing) to analyze 42 neuroblastoma cell lines by CGH analysis. This study provided detailed mapping of shortest regions of overlap for many recurrent genomic imbalances and identification of novel abnormalities that were too subtle to detect by metaphase CGH. Although homozygous deletion of tumor suppressor gene regions have been noted at high frequency in several different tumor types (10), the array CGH study of Mosse et al. (8) identified only a single region of homozygous deletion, a 9.3-Mb region on chromosome 3p. Recently, we (11) showed the utility of oligonucleotide array CGH for mapping unbalanced chromosomal breakpoints and identifying subtle chromosomal imbalances at resolutions ranging from <1 kb (focused fine tiling arrays) to ~25 kb (whole-genome arrays). The arrays contain up to 390,000 repeat masked oligonucleotides. Here, we report on the first major application of this oligonucleotide array CGH technology for high-resolution mapping of unbalanced chromosome breakpoints and identification of subtle chromosomal imbalances in a large set of human neuroblastoma primary tumors and cell lines. These results allow a global view of genomic instability at exon-level resolution and the identification of gene loci that are recurrently deleted.

Materials and Methods

DNA samples from primary tumors were obtained from several sources, including the Children's Oncology Group Tumor Bank (Philadelphia, PA), a

Note: Supplementary data for this article are available at Cancer Research Online (<http://cancerres.aacrjournals.org/>).

Requests for reprints: Raymond L. Stallings, Children's Cancer Research Institute and Department of Pediatrics, University of Texas Health Science Center at San Antonio, 8403 Floyd Curl Drive, Mail Code 7784, San Antonio, TX 78229-3900. Phone: 210-562-9028; Fax: 210-562-9014; E-mail: Stallings@uthscsa.edu.

©2006 American Association for Cancer Research.
doi:10.1158/0008-5472.CAN-05-4154

tumor bank at Our Lady's Hospital for Sick Children (Dublin, Ireland), and the Children's Hospital at Westmead (Sydney, New South Wales, Australia). Tumors used in this study were selected based on either having loss of 11q material or *MYCN* amplification, which define the two most common genetic subtypes of stage IV disease. The abnormalities identified in this study are therefore not representative of the entire neuroblastoma population. Samples from the Our Lady's Hospital for Sick Children and Children's Hospital at Westmead were characterized previously for large-scale chromosomal imbalances by metaphase CGH analysis (12–15), whereas samples from the Children's Oncology Group have been analyzed for loss of 11q by allotyping with several different polymorphic loci (6). *MYCN* amplification status in each sample was also assessed by either fluorescence *in situ* hybridization, Southern blotting, or quantitative PCR. Oligonucleotide array CGH results for three tumors (31, 37, and 47) and two cell lines (SK-N-AS and Kelly/N206) have been reported previously (11).

Oligonucleotide array CGH was carried out by NimbleGen Systems, Inc., at their facility in Iceland. Methods of DNA labeling, array construction, and hybridization as well as methods for array normalization and data analysis have been described in detail by Selzer et al. (11). Briefly, the whole-genome array incorporates 390,000 oligonucleotides (median probe spacing of 6 kb) from unique sequence regions that are of variable length to achieve a melting temperature of 76°C. Total genomic DNA from each tumor is directly labeled by random primer extension labeling (Cy3) without an intervening whole-genome amplification step (11). A matched reference DNA from the cancer patient was used as the reference DNA (labeled with Cy5) in a limited number of instances (tumors 178, 439, and 1389). Nonmatched reference DNAs were from a pool of six male individuals (Promega, Madison, WI). Data were analyzed using both unaveraged probes and by window averaging (25- and 50-kb window sizes) as described previously (11). In all instances, DNA sequence coordinates are from National Center for Biotechnology Information Build 35.

Methods for validating oligonucleotide array CGH results using real-time quantitative PCR have been described in detail by Selzer et al. (11). The single-copy loci *GAPDH* or *ACTB* were used for normalization. Primer sequences for each sequence-tagged site marker used in Fig. 4 can be obtained using the University of California at Santa Cruz Genome Browser tool.⁶

Results

Analysis of breakpoints leading to large-scale chromosomal imbalances. CGH analysis of 49 primary neuroblastoma tumors, 1 matched metastatic tumor, and 6 cell lines (SK-N-AS, Kelly/N206, SK-N-BE, IMR32, NGP, and NB69) was carried out using a whole-genome oligonucleotide microarray with a median probe spacing of 6 kb. A total of 467 independent chromosome breakpoints were identified that led to the generation of 416 partial chromosome imbalances >2 Mb long. Each breakpoint could be mapped to intervals ranging in size from 6 to 50 kb (breakpoint positions obtained primarily by 25-kb window averaging are listed in Supplementary Table S1). The distribution of the breakpoints was bimodal, with tumors tending to have either very few breakpoints (<5) or a large number (>15). Sixty-four whole chromosome gains or losses were also detected so that the total number of imbalances >2 Mb was 480.

There was a strong correlation between large-scale chromosomal imbalances (>10 Mb) detected by oligonucleotide array CGH and prior metaphase CGH analyses. However, oligonucleotide array CGH detected many imbalances <10 Mb that were not detected by metaphase CGH. There was also substantial consistency between loss of 11q detected by allotyping studies and oligonucleotide array CGH analysis, except for tumors 178, 151, and 1389. These three

tumors were determined to have 11q loss by allotyping but not by oligonucleotide array CGH. A likely explanation for the inconsistency is that the event leading to loss of 11q heterozygosity was a copy neutral change, perhaps resulting from gene conversion or mitotic recombination (i.e., loss of one set of alleles and reduplication of the remaining set).

Chromosome 11q breakpoint positions ranged from coordinates 65.5 to 114.2 Mb among the 32 tumors or cell lines that had hemizygous loss of 11q. Fifty-six percent of these breakpoints clustered within a 4-Mb region between coordinates 68 and 72 Mb. Smaller clusters of breakpoints mapped between coordinates 80 and 85 Mb (19%) and to a narrow 260-kb interval between 98.775 and 99.03 Mb (9%) containing the *CNTN5* locus. The most distal breakpoint at 114.2 Mb occurred in the *MYCN* amplified Kelly/N206 cell line. This abnormality may reflect a random, secondary alteration, so that the region 98 Mb to qter more likely represents the candidate tumor suppressor gene(s) region on 11q.

Ten of the 32 (31%) chromosome 11q breakpoint intervals leading to 11q loss contained segmental duplications (50-kb intervals assigned by 25-kb window averaging). From Armengol et al. (16), we were able to ascertain that the expected frequency of segmental duplications occurring within randomly placed 50-kb intervals on chromosome 11 is only 15%, allowing us to conclude that our observed frequency is significantly higher than would be expected by random chance. Five of the 11q breakpoints mapped within a narrow 225-kb interval (71037500-71262500 bp) covered by segmental duplications, further supporting the concept that 11q breakpoints are nonrandomly associated with segmentally duplicated regions.

Fifty breakpoints leading to gain of chromosome 17q were identified, with some tumors having multiple regions of 17q gain. Eighty percent of 17q breakpoints mapped to an 18-Mb interval between coordinates 27 and 45 Mb. Sixteen of 50 (32%) chromosome 17q breakpoint intervals mapped to segmentally duplicated regions, which is only slightly greater than would be expected (31%) based on the overall frequency of segmental duplications on this chromosome.

Twenty-seven breakpoints leading to loss of chromosome 3p could be identified, some of which involved interstitial loss of 3p material rather than terminal deletion. Seventy percent of 3p breakpoints mapped to a 20-Mb interval between coordinates 48 and 68 Mb. Clustering of 3p breakpoints was less evident than for either 17q or 11q, and none of the 27 breakpoints leading to 3p loss contained segmental duplications.

Analysis of the remaining 358 breakpoints leading to imbalances >2 Mb indicated that 59 (16%) were associated with segmental duplications, which is not significantly different from what would be expected by random chance (expected = 18% based on ref. 16).

Analysis of high-level amplification. Eighteen tumors or cell lines had high-level amplification of the *MYCN* locus at 2p24 (\log_2 ratio ≥ 2.0). High-level amplification also occurred at 18 chromosome 2 regions that were discontinuous with the *MYCN* locus and located at varying distances from *MYCN* (Supplementary Table S2). The level of amplification and number of distinct sites amplified in a tumor were highly variable. Some cases, such as the cell line SK-N-BE, possessed a single, contiguous region of amplification encompassing the *MYCN* gene (Fig. 1A). The majority of tumors, however, possessed amplifications of the *MYCN* region and other high-level amplifications on chromosome 2 that were noncontiguous with the *MYCN* amplicon. The additional amplification events were sometimes in close proximity to the *MYCN*

⁶ <http://genome.cse.ucsc.edu/>.

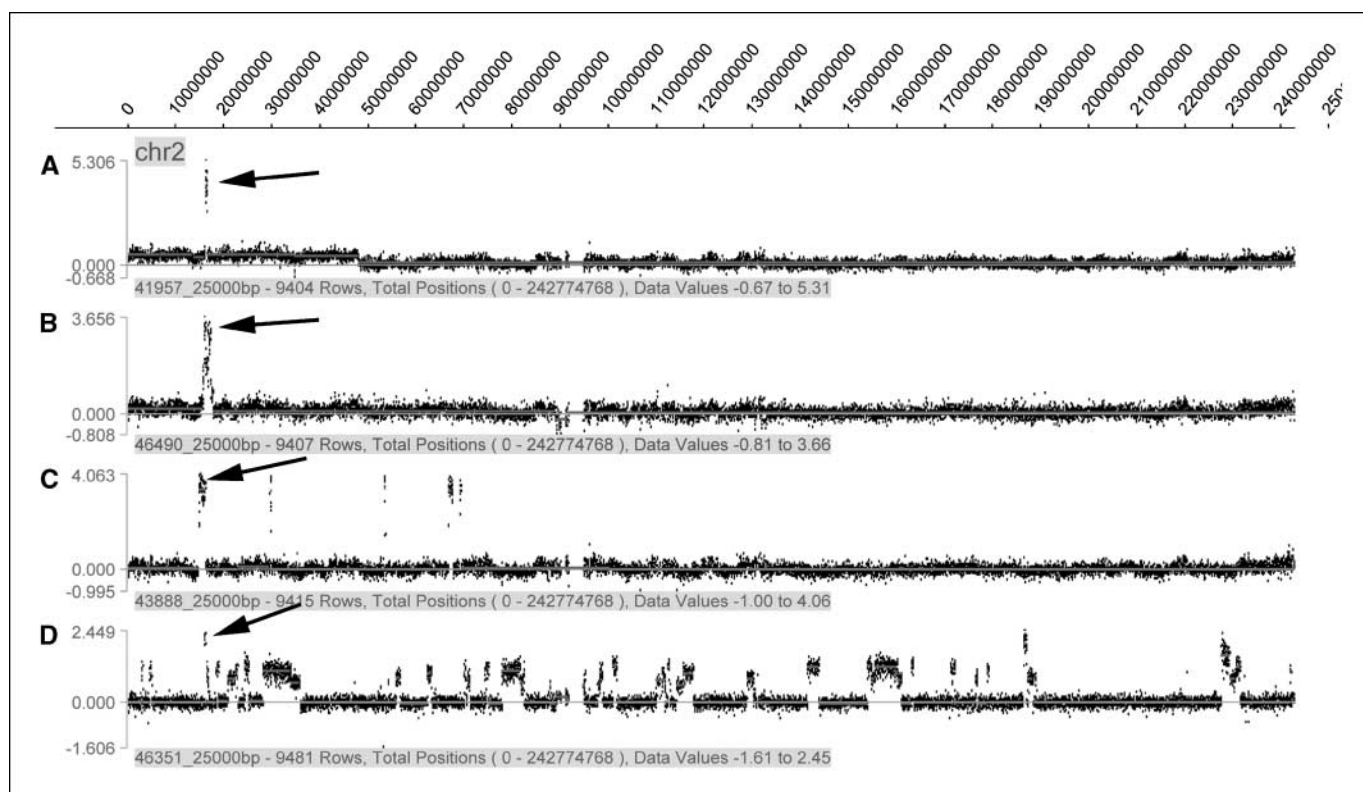


Figure 1. Examples of *MYCN* amplification detected by oligonucleotide array CGH analysis (25-kb window averaging) visually depicted with the SignalMap graphical interface tool from NimbleGen Systems. Arrows, *MYCN* region. A, amplification in the cell line SK-N-BE was a simple continuous region of amplification. B, tumor 86 had three distinct regions of high-level amplification separated by relatively short distances along with lower-level gains. C, IMR32 had six distinct regions of high-level amplification, which were separated by considerable distance (except for the two most distal amplicons). D, tumor T1068 had one region of high-level amplification and >30 regions of lower-level gain (\log_2 ratio > 0.7) along the length of chromosome 2.

locus (Fig. 1B), and in some instances, many megabases distant from this locus (Fig. 1C). Low-level gain of chromosome 2 regions that were interspersed between regions of high-level amplification were common. The most extreme example of moderate-level gains along the entire length of chromosome 2 occurred in tumor 1068, which had 36 distinct genomic regions with \log_2 ratios exceeding 0.7 (Fig. 1D).

Three of the tumors possessing *MYCN* amplification also had high-level amplification of other chromosomal regions, including 11q13 (*CCND1*) in tumor 86 and 12q24 (*MDM2*) in tumor 6 and NGP. Both *CCND1* and *MDM2* amplification have been noted previously in neuroblastoma (17, 18). There were also additional sites of high level of amplification on chromosomes 11 and 12 that were discontinuous with *CCND1* and *MDM2* (Supplementary Table S2).

Analysis of breakpoints leading to small-scale chromosomal imbalances. Imbalances ($n = 540$) that were <2 Mb long, ranging from 0.025 to 1.3 Mb in size, were detected. It is unlikely that these subtle imbalances are technical artifact because no imbalances were observed using the same analysis criteria in three experiments where normal DNA from the same individual was used as both test and reference DNA (11).

The recent discovery of large-scale, widespread copy number polymorphisms (CNP) at segmentally duplicated loci (19, 20), however, suggests that many of these smaller-scale imbalances represent constitutional copy number differences between test and reference genomes. This possibility was tested by examining the sequences present at each imbalance with the University of California at Santa Cruz Genome Browser tool.⁶ We ascertained

that 383 of these variants mapped to regions containing segmental duplications and therefore might reflect CNPs. In addition, 38 imbalances, which did not overlap segmentally duplicated regions, corresponded to known CNPs listed in the Database of Genomic Variants.⁷ Therefore, 421 (78%) of the imbalances <2 Mb long are potentially normal constitutional variants. The use of a matched constitutional DNA sample as the reference for three tumors strongly suppressed the appearance of subtle variants in those tumors, further indicating that the majority of subtle imbalances represent germ-line copy number differences between the patient DNA and the reference DNA (pooled from six normal males).

Not all imbalances at segmentally duplicated loci, however, were suppressed by the use of a matched constitutional reference DNA, indicating that some imbalances are somatic events. In several instances, we found that large-scale chromosomal gains or losses that include duplicated loci could lead to the "appearance" of imbalance in other regions that possess homology to the segmental duplications. For example, tumor 1359 had gain of a large region on chromosome 7q (69.96-107.76 Mb) that included a small region that is duplicated on chromosome 1p between 83.337 and 83.662 Mb. As shown in Fig. 2, gain of the large segment of 7q resulted in the appearance of gain over a small 325-kb region of chromosome 1p (83.337-83.662 Mb) and over a 500-kb region on 7q (75.762-76.262 Mb) that has homology to the 1p region and other sites on 7q. Although we cannot rule out the possibility that copy number

⁷ <http://projects.tcag.ca/variation/>.

polymorphic differences contributed to the imbalance, CNPs do not have to be invoked to explain these effects. These types of effects were noted for several other genomic regions.

The remaining 119 imbalances that were <2 Mb long did not map to segmentally duplicated regions and were not listed as CNPs in the Database of Genomic Variants. Fifty-nine of these 119 imbalances mapped to either intergenic regions or predicted gene sequences of unknown function. The significance of these imbalances remains to be determined. Sixty imbalances mapped to regions containing characterized genes, many of which play roles in tumorigenesis, apoptosis, or neural cell differentiation (Table 1). The most frequent region of recurrent microdeletion involved the *PTPRD* gene region at chromosome 9p23 in three cell lines (NGP, Kelly, and SK-N-AS) and three tumors (31-MAR, 430, and 47). The deletions included either *PTPRD* coding exons (NGP, metastatic tumor 31-MAR, and tumor 430) or exons from the 5' untranslated region (UTR; tumor 47, Kelly, and SK-N-AS). We also found one tumor (1173) with an unbalanced chromosome 9p breakpoint that disrupted the 5' UTR of *PTPRD*. Chromosome 9p deletions, along with a deletion map of the *PTPRD* locus, are illustrated in Fig. 3.

The *PTPRD* deletion in 31-MAR was clearly somatically acquired because 31-MAR represents a metastatic bone marrow aspirate (Fig. 3A) and the deletion was not present in material from the primary tumor (Fig. 3B). Real-time quantitative PCR analysis of primary tumor DNA and a matched constitutional DNA from case 430 also confirmed that the deletion was somatically acquired in the tumor from this patient (Fig. 4A).

In the Kelly/N206 cell line, two different shifts in log₂ ratio were detected, indicating that part of the *PTPRD* region is homozygously deleted. As illustrated in Fig. 4B, real-time quantitative PCR analysis with primers from the putative homozygously deleted region generated primer product that was significantly lower than would have been expected for only hemizygous loss, thus

confirming homozygous loss. The SK-N-AS cell line had large-scale loss of the majority of 9p as well as a further decrease in the log₂ ratio for a small region of *PTPRD*, also indicative of homozygous loss. Real-time quantitative PCR analysis of SK-N-AS with primers from the undeleted region, the region of hemizygous loss, and the putative homozygously deleted region was consistent with homozygous deletion in a subpopulation of cells (Fig. 4C).

Discussion

The exon-level resolution mapping of unbalanced chromosomal breakpoints accomplished in this study helps narrow down the regions harboring potential neuroblastoma oncogenes or tumor suppressor genes. At the same time, these experiments provide information on the sequences found in proximity to the breakpoints, which can facilitate our understanding of the events that generate recurrent chromosomal imbalances. Breakpoints leading to 11q loss in neuroblastoma cells were more clustered than breakpoints on other chromosomes and contained segmental duplications at a higher than expected frequency, indicating that the duplications play a role in generating 11q breakpoints. Thus, it seems likely that the mechanism generating 11q loss in many instances is quite different from the mechanisms generating other chromosomal imbalances. In this regard, we note that loss of 11q occurs primarily through a common chromosomal mechanism, an unbalanced t(11;17) (ref. 15), whereas the mechanisms leading to many other recurrent abnormalities, except for loss of 1p which is due to a t(1;17), are more variable. The segmental duplications found at the 11q breakpoints, however, are not duplicated within the defined 17q breakpoint intervals, indicating that they have not caused inappropriate homologous recombination to occur. The precise molecular mechanisms generating this translocation require further studies.

The detection of a complex series of highly amplified regions that are discontinuous with *MYCN* and interspersed with regions of

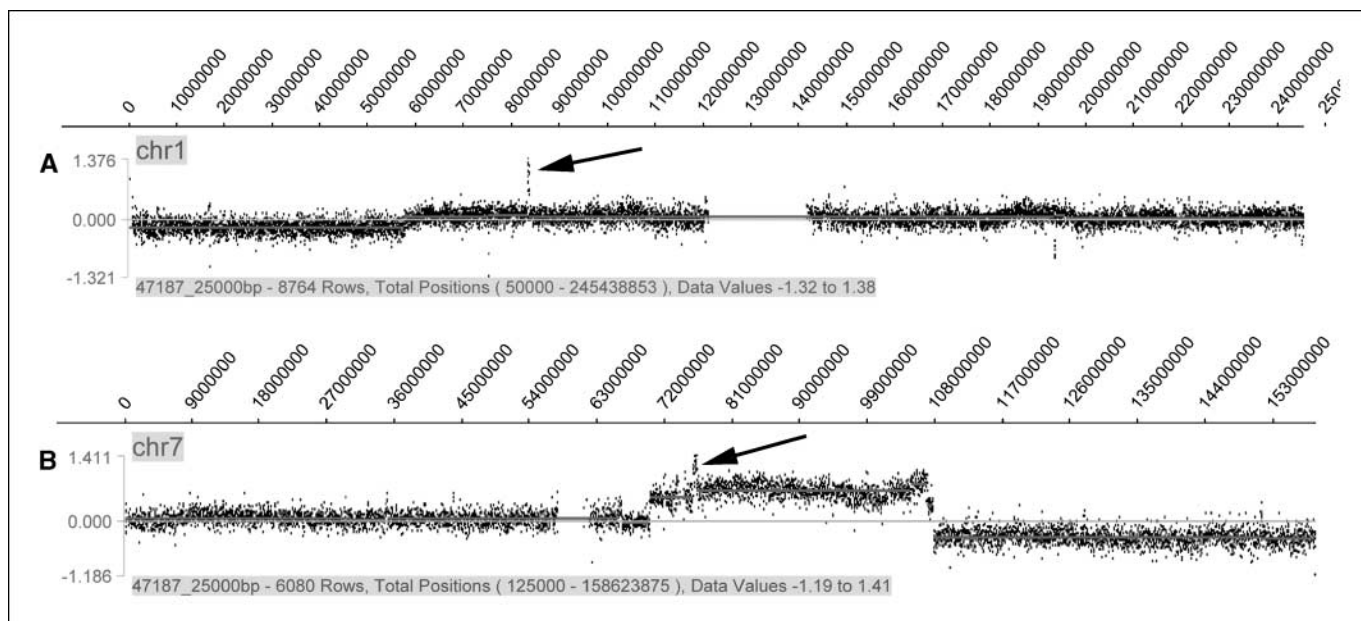


Figure 2. A, 325-kb region of apparent gain on chromosome 1p at 83337500 to 83662500 bp (arrow) in tumor 1359 is the consequence of large-scale gain on chromosome 7q from 75762500 to 76262500 bp. B, region of large-scale gain on 7q encompasses a duplicated region from 75762500 to 76262500 bp (arrow) that has homology to the region on 1p and to other regions on 7q. The region on 7q with homology to 1p also shows a level of gain greater than that displayed for the region of large-scale gain. Thus, large-scale gain of 7q has led to an increase in the number of copies that have homology to the chr1:3337500-83662500 and chr7:75762500-76262500 regions, leading to the appearance of gain at both microregions (arrows).

Table 1. Imbalances <2 Mb mapping to known genes

Sample	Band	Coordinates	Size (Mb)	Genes
1043	dim +1p36.23	7162500-7337500	0.2	<i>CAMTA1</i>
1220	dim 1p36.21	13675000-14675000	0.100	<i>PRDM2</i>
34	enh 1p31.2	66437500-66987500	0.55	<i>PDE4B; BC040416</i>
1128	enh 1p36.22	11612500-11687500	0.075	<i>MAD2L2; FBX06; FBX044</i>
6	dim p21.3	96787500-97037500	0.275	<i>PTPB2</i>
NGP	enh +1q23.1	153537500-153812500	0.3	<i>NTRK1; PRCC</i>
6	enh 1q23.3	159737500-159987500	0.275	<i>RGS4; RGS5</i>
NGP	enh 1p33-p32.3	50387500-52037500	1.675	<i>RET1</i> + additional genes
NGP	enh +2p22.2-p22.1	37337500-38587500	1.275	Several genes
10	enh 2q22.1	141175000-142375000	1.2	<i>LRP1B</i>
NGP	enh 3q13.31	166762500-117087500	0.35	<i>GAP43</i>
Kelly	dim 3q13.31	117137500-118087500	0.950	<i>LSAMP</i>
SK-N-AS	dim 3q13.31	117037500-117487500	0.450	<i>LSAMP</i>
44	dim 3p24.3	17387500-17437500	0.05	<i>TBC1D5</i>
1043	enh 3p21.21	48037500-48512500	0.5	<i>CDC25A</i> + additional genes
86	enh 4q31.1	140587500-141912500	1.3	<i>NARG1; RAB33B; SET7</i>
42	enh 4p14	39262500-39387500	0.125	<i>LIAS; RPL9UGDH</i>
136	dim 4p12	48012500-48137500	0.125	<i>TEC</i>
22	enh 4q32.21	143387500-143412500	0.025	<i>INPP4B</i>
NGP	enh +4q34.1	175112500-175537500	0.425	<i>FBX08</i>
6	enh 5q11.2	57762500-58262500	0.525	<i>RAB3C</i>
10	enh 5q12.1	60125000-60875000	0.75	<i>ERCC8</i>
NGP	enh 5q32	145462500-145637500	0.2	<i>LARS</i>
42	dim 5q33.1	150162500-150287500	0.125	<i>ZNF300</i>
42	enh 6p21.1	42987500-43112500	0.125	<i>PPP2R5D</i> + additional genes
NGP	enh 6q22.1	116037500-117187500	1.175	<i>FRK</i>
283	dim 6q27	168162500-168412500	0.25	<i>KIF25</i>
1068	enh 6q27	168162500-168437500	0.275	<i>KIF25</i>
1126	enh 6q27	168162400-168387500	0.225	<i>KIF25</i>
1043	dim 7pter-p22.3	0.137-1.237	0.9	Several genes
IMR32	dim 7q35-q36.1	146787500-147762500	0.975	<i>CNTNAP2</i>
1068	enh 7q35	144562500-145437500	0.875	<i>CNTNAP2</i>
10	dim 7q35-q36.1	146225000-147525000	1.3	<i>CNTNAP2</i>
Kelly	dim 7q35	146387500-146512500	0.125	<i>CNTNAP2</i>
47	enh 7q32.1	131637500-132412500	0.775	<i>CH3HD3</i>
40	dim 7q21.3	94375000-94475000	0.1	<i>PPP1R9A</i>
47	dim 8p23.1	9225000-10075000	0.85	<i>TNKS</i>
45	enh 8p21.3	21987500-22112500	0.875	<i>RAI16</i> + additional genes
47	dim 9p23	9262500-10087500	0.825	<i>PTPRD; NRG2</i>
31-mar	dim 9p24.1-p23	8537500-9262500	0.725	<i>PTPRD</i>
Kelly	dim 9p23	9212500-9737500	0.515	<i>PTPRD</i>
T430	dim 9p24.1-p23	8987500-9162500	0.175	<i>PTPRD</i>
SK-N-AS	dim 9p23	9200000-9675000	0.475	<i>PTPRD</i>
NGP	dim 9p24.1-p23	8487500-9262500	0.8	<i>PTPRD</i>
1173	dim 9p21.3	23637500-23762500	0.125	<i>ELAVL2</i>
NGP	enh 9q22.32	96087500-96487500	0.425	<i>CDC14B</i>
34	enh 10p14	8087500-8387500	0.3	<i>GATA3</i>
SK-N-AS	dim 10q24.31	102312500-102912500	0.6	<i>PAX2; SEMA4G; TLX1</i>
SK-N-AS	dim 11q22.1	99462500-99537500	0.075	<i>CNTN5</i>
86	enh 12p13.33	2984373-3490627	0.506	<i>TSPAN9</i>
283	dim 12q23.1	97462500-97937500	0.475	<i>APAF1</i>
493	dim 12q23.1	97462500-98987500	1.55	<i>APAF1</i> + additional genes
430	enh 12q24.12	110662500-110762500	0.1	<i>ALDH2; MAPKAPK5</i>
14	enh 14q13.2	35062500-35537500	0.475	<i>GARNL1</i>
6	enh 14q24.3	77087500-77137500	0.075	<i>SPTLC2</i>
44	dim 16p13.3	3737500-3812500	0.075	<i>CREBBP</i>
Kelly	dim 16p13.3-p13.2	6237500-6887500	0.650	<i>A2BP1</i>
1173	dim 17p11.2	18887500-19962500	1.075	<i>MAPK7</i>
86	dim 17p13.2	4112500-4187500	0.075	<i>UBE2G1</i>
86	enh 19p13.2	47362500-47612500	0.25	<i>DEDD2</i>

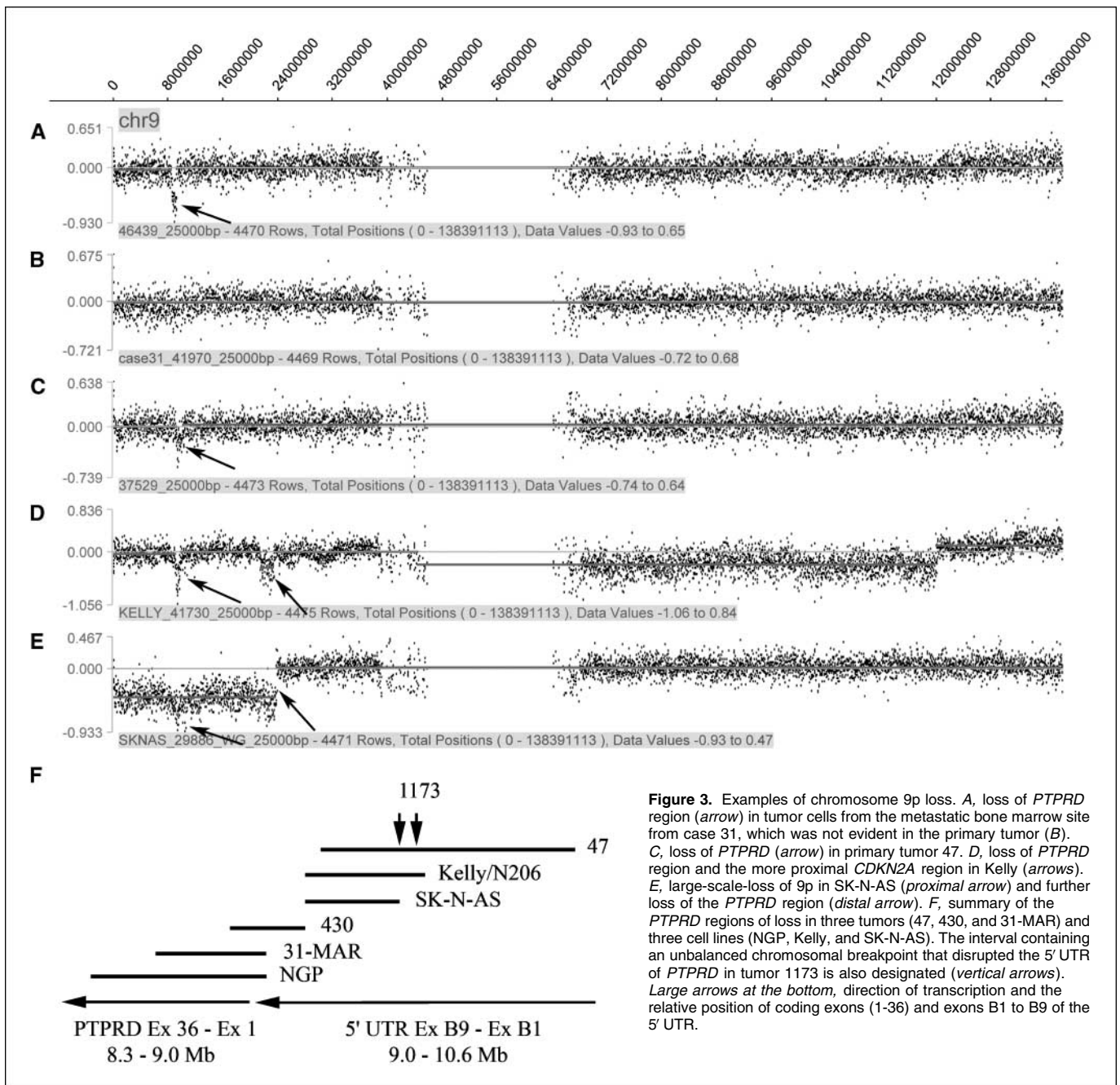


Figure 3. Examples of chromosome 9p loss. *A*, loss of *PTPRD* region (arrow) in tumor cells from the metastatic bone marrow site from case 31, which was not evident in the primary tumor (*B*). *C*, loss of *PTPRD* (arrow) in primary tumor 47. *D*, loss of *PTPRD* region and the more proximal *CDKN2A* region in Kelly (arrows). *E*, large-scale-loss of 9p in SK-N-AS (proximal arrow) and further loss of the *PTPRD* region (distal arrow). *F*, summary of the *PTPRD* regions of loss in three tumors (47, 430, and 31-MAR) and three cell lines (NGP, Kelly, and SK-N-AS). The interval containing an unbalanced chromosomal breakpoint that disrupted the 5' UTR of *PTPRD* in tumor 1173 is also designated (vertical arrows). Large arrows at the bottom, direction of transcription and the relative position of coding exons (1-36) and exons B1 to B9 of the 5' UTR.

lower-level gains is consistent with earlier studies by Shiloh et al. (21). The oligonucleotide array CGH analyses carried out in our study, however, provide substantially higher-resolution mapping of amplicon boundaries than what has heretofore been carried out.

The extremely high-resolution achievable by oligonucleotide array CGH analysis, although a major strength, is also a weakness because of the present difficulties associated with distinguishing pathologically important imbalances from those that are simply due to the high level of genomic instability that is characteristic of most tumors. The imbalances detected at segmentally duplicated loci often reflect constitutional copy number differences between tumor and reference DNA sample from different individuals as observed in several studies (19, 20). Our results indicate that the

use of a matched constitutional DNA sample from the patient as the reference DNA sample does not completely eliminate the appearance of small imbalances at segmentally duplicated loci. In some instances, the appearance of subtle imbalances at segmentally duplicated regions is caused by the large-scale losses or gains of regions containing segmental duplications that are homologous to the subtle region where imbalance is detected. These intra-chromosomal/interchromosomal "long distance" effects are easily traceable and should be taken into account when interpreting high-resolution oligonucleotide array CGH data. Although use of a matched constitutional reference DNA sample suppresses the appearance of the majority of CNP variants, matched samples are not always available for rare pediatric tumors. The development of

a comprehensive CNP database should be very helpful for distinguishing between normal variants and somatic abnormalities found in some tumors.

We had an expectation of finding homozygous deletions for the 11q region in neuroblastoma given that homozygous deletions have been identified at high frequency in cell lines from many different tumor types (e.g., ref. 10). However, consistent with the BAC array CGH study of Mosse et al. (8), we have found that recurrent homozygous deletions are exceedingly rare in neuroblastoma. Apart from a previously reported 67-kb homozygous deletion of an intronic region of *CNTN5* (11), no homozygous loss on chromosome 11q could be detected in any of the 32 tumors and cell lines that possessed large-scale hemizygous loss of this chromosomal region. Interestingly, the breakpoint resulting in

large-scale hemizygous loss of 11q disrupted the *CNTN5* locus in two primary tumors (1100 and 23) and one cell line (NGP). *CNTN5* is a glycosylphosphatidylinositol-anchored neuronal membrane protein that mediates cell surface interactions during nervous system development. Further studies are required to determine if this region is simply a hotspot for breakage or whether disruption of this gene plays a role in neuroblastoma pathogenesis.

The lack of homozygous deletions on chromosome 11q could mean that a tumorigenic effect is being rendered through haploinsufficiency of one or more genes on 11q. In this regard, there are two genes on chromosome 11q involved with genomic stability (*ATM* and *H2XA*) that may have a tumorigenic effect through a haploinsufficient mechanism (see ref. 22 for review). A

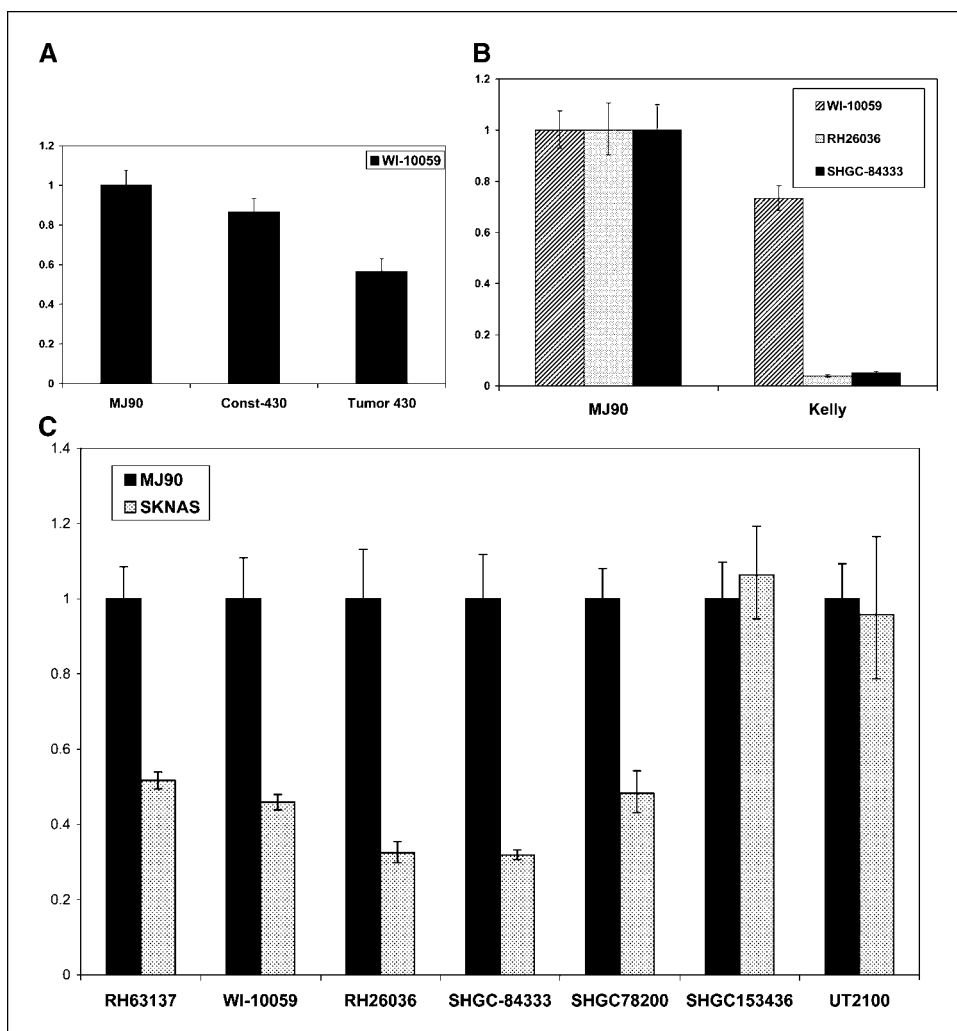


Figure 4. Validation of *PTPRD* deletions with real-time quantitative PCR. **A**, primer WI-10059, mapping to the deleted region in tumor 430, shows no decrease in PCR product in a constitutional DNA sample from patient 430 relative to DNA from a normal fibroblast cell line (MJ90). There was a significant decrease in PCR product in tumor DNA relative to the constitutional DNA sample and normal fibroblast sample, confirming the presence of a somatically acquired deletion. **B**, validation of *PTPRD* deleted region in Kelly. Primer WI-10059 maps outside the deleted region, whereas primers RH26036 and SHGC-84333 map within the region determined to be deleted by CGH. There is an ~20 fold decrease in RH26036 and SHGC-84333 PCR product relative to WI-10059. We conclude that the region is homozygously deleted in Kelly because this decrease is substantially larger than the 50% reduction that would be caused by a hemizygous deletion. **C**, validation of deletion in SK-N-AS. Primers RH63137 and WI-10059 map within the region of large-scale hemizygous 9p loss but distal to the smaller region of homozygous loss. Primers RH26036 and SHGC-84333 map within the putative region of homozygous loss, whereas SHGC-78200 maps outside this region but within the region of hemizygous loss. The remaining primers SHGC-153436 and UT2100 map proximal of the region of hemizygous loss (i.e., not deleted). Both RH26036 and SHGC-84333 show less PCR product than the primers mapping only to the region of hemizygous loss, consistent with homozygous loss of this region in some cells. The level of PCR amplification of each of these primers suggests, however, that only a subpopulation of cells possesses the homozygous deletion. All primer sequences and map positions can be found using the University of California at Santa Cruz Genome Browser.⁹ Amount of PCR product is relative to MJ90, a normal human fibroblast cell line.

simple model for the development of the 11q– neuroblastoma subtype would involve simultaneous loss of 11q and gain of 17q through an unbalanced t(11;17). Perhaps hemizygous loss of critical genes involved with maintenance of genomic integrity on 11q, such as *ATM* and *H2XA*, coupled with gain of antiapoptotic sequences, such as *BIRC5* and *miR-21*, on 17q, leads to an early-stage tumor. Loss of 11q and gain of 17q were the sole imbalances detected in one tumor, which supports the notion that these are early events. In addition, expression microarray analysis of 11q– neuroblastomas has shown that rare low-stage 11q– tumors sometimes have global gene expression profiles that are much more similar to low-stage hyperdiploid tumors than to high-stage 11q– tumors, an indication that loss of 11q and gain of 17q are insufficient for the establishment of metastasis (13). It is tempting to speculate that some of the microdeletions and duplications listed in Table 1 contribute to the establishment of metastatic potential in neuroblastoma; however, the possibility that many of them are merely a consequence of global genomic instability cannot be ruled out. Additional studies are required to confirm any role that these subtle abnormalities might play in neuroblastoma pathogenesis.

One of the more important events for the development of metastatic neuroblastoma might be loss of *PTPRD*, which occurred in ~12% of our samples. *PTPRD* seemed to be homozygously deleted in two neuroblastoma cell lines and is also commonly homozygously deleted in lung cancer (23–25),

suggesting that it plays a fundamental role in cancer development. It was recently determined that two mRNA isoforms of *PTPRD* exist, one containing a long 5' UTR (L form) and a second without the 5' UTR (S form; ref. 24). This gene cooperates with the *MIM* gene to induce cytoskeletal changes (26). It has been suggested that deletions occurring in the *PTPRD* locus could represent some kind of region-specific hotspot for rearrangement (24), given that large-scale inversions and duplications non-randomly occur in this region in lymphocytes of *BRCA2* mutation carriers (27). However, neither neuroblastoma or lung cancer patients are likely to have constitutional mutations in *BRCA2*, and the large-scale duplications and inversions on chromosome 9 are quite different from the subtle somatically acquired deletions. A role for *PTPRD* in cancer seems plausible, given that other protein tyrosine phosphatase receptors play important roles in tumorigenesis (28–30). Ascertaining the possible functional effects that deletions of the 5' UTR might have on either transcription or translation of *PTPRD* should shed considerable light on this issue.

Acknowledgments

Received 11/18/2005; revised 1/11/2006; accepted 2/1/2006.

Grant support: Children's Medical and Research Foundation (Dublin, Ireland).

The costs of publication of this article were defrayed in part by the payment of page charges. This article must therefore be hereby marked *advertisement* in accordance with 18 U.S.C. Section 1734 solely to indicate this fact.

References

- Brodeur GM. Neuroblastoma: biological insights into a clinical enigma. *Nat Rev Cancer* 2003;3:203–16.
- Brodeur GM, Seeger RC, Schwab M, Varmus HE, Bishop JM. Amplification of N-myc in untreated human neuroblastomas correlates with advanced disease stage. *Science* 1984;224:1121–4.
- Bown N, Cotterill S, Lastowska M, et al. Gain of chromosome arm 17q and adverse outcome in patients with neuroblastoma. *N Engl J Med* 1999;340:1954–61.
- Spitz R, Hero B, Ernestus K, Berthold F. Deletions in chromosome arms 3p and 11q are new prognostic markers in localized and 4s neuroblastoma. *Clin Cancer Res* 2003;9:52–8.
- Vandesompele J, Baudis M, De Preter K, et al. Unequivocal delineation of clinicogenetic subgroups and development of a new model for improved outcome prediction in neuroblastoma. *J Clin Oncol* 2005;23:2280–99.
- Guo C, White PS, Weiss MJ, et al. Allelic deletion at 11q23 is common in MYCN single copy neuroblastomas. *Oncogene* 1999;18:4948–57.
- Plantaz D, Vandesompele J, Van Roy N, et al. Comparative genomic hybridization (CGH) analysis of stage 4 neuroblastoma reveals high frequency of 11q deletion in tumors lacking MYCN amplification. *Int J Cancer* 2001;91:680–6.
- Mosse YP, Greshock J, Margolin A, et al. High resolution detection and mapping of genomic DNA alterations in neuroblastoma. *Genes Chromosomes Cancer* 2005;43:390–403.
- Chen QR, Bilke S, Wei JS, et al. cDNA array-CGH profiling identifies genomic alterations specific to stage and MYCN-amplification in neuroblastoma. *BMC Genomics* 2004;5:1–13.
- Senchenko VN, Liu J, Loginov W, et al. Discovery of frequent homozygous deletions in chromosome 3p21.3 LUCA and AP20 regions in renal, lung and breast carcinomas. *Oncogene* 2004;23:5719–28.
- Selzer RR, Richmond TA, Pofahl NJ, et al. Analysis of chromosome breakpoints in neuroblastoma at sub-kilobase resolution using fine tiling oligonucleotide array CGH. *Genes Chromosomes Cancer* 2005;44:305–19.
- Breen CJ, O'Meara A, McDermott M, Mullarkey M, Stallings RL. Co-ordinate deletion of chromosome 3p and 11q in neuroblastoma detected by comparative genomic hybridization. *Cancer Genet Cytogenet* 2000;120:44–9.
- McArdle L, McDermott M, Purcell R, et al. DNA microarray analysis of gene expression in neuroblastoma displaying loss of 11q. *Carcinogenesis* 2004;25:1599–609.
- Stallings RL, Howard J, Dunlop A, et al. Are gains of chromosomal regions 7q and 11p important abnormalities in neuroblastoma? *Cancer Genet Cytogenet* 2003;140:133–7.
- Stallings RL, Carty P, McArdle L, et al. Molecular cytogenetic analysis of recurrent unbalanced t(11;17)s in neuroblastoma. *Cancer Genet Cytogenet* 2004;154:44–51.
- Armengol L, Pujana MA, Cheung J, Scherer SW, Estivill X. Enrichment of segmental duplications in regions of breaks of synteny between the human and mouse genomes suggest their involvement in evolutionary rearrangements. *Hum Mol Genet* 2003;12:2201–8.
- Molenaar JJ, van Sluis P, Boon K, Versteeg R, Caron HN. Rearrangements and increased expression of cyclin D1 (CCND1) in neuroblastoma. *Genes Chromosomes Cancer* 2003;36:242–9.
- Corvi R, Savelyeva L, Amler L, Handgretinger R, Schwab M. Cytogenetic evolution of MYCN and MDM2 amplification in the neuroblastoma LS tumour and its cell line. *Eur J Cancer* 1995;31A:520–3.
- Sebat J, Lakshmi B, Troge J, et al. Large-scale copy number polymorphism in the human genome. *Science* 2004;305:525–8.
- Iafraite AJ, Feuk L, Rivera MN, et al. Detection of large-scale variation in the human genome. *Nat Genet* 2004;36:949–51.
- Shiloh Y, Korf B, Kohl NE, et al. Amplification and rearrangement of DNA sequences from the chromosomal region 2p24 in human neuroblastomas. *Cancer Res* 1986;46:5297–301.
- Santarosa M, Ashworth A. Haploinsufficiency for tumour suppressor genes: when you don't need to go all the way. *Biochim Biophys Acta* 2004;1654:105–22.
- Cox C, Bignell G, Greenman C, et al. A survey of homozygous deletions in human cancer genomes. *Proc Natl Acad Sci U S A* 2005;102:4542–7.
- Sato M, Takahashi K, Nagayama K, et al. Identification of chromosome 9p as the most frequent target of homozygous deletions in lung cancer. *Genes Chromosomes Cancer* 2005;44:405–14.
- Zhao X, Weir BA, LaFramboise T, et al. Homozygous deletions and chromosome amplifications in human lung carcinomas revealed by single nucleotide polymorphism array analysis. *Cancer Res* 2005;65:5561–70.
- Gonzalez-Quevedo R, Shoffer M, Hornig L, Oro AE. Receptor tyrosine phosphatase-dependent cytoskeletal remodeling by the hedgehog-responsive gene *MIM/BEG4*. *J Cell Biol* 2005;168:453–63.
- Savelyeva L, Claas A, Matzner I, et al. Constitutional genomic instability with inversions, duplications, and amplifications in 9p23-24 in *BRCA2* mutation carriers. *Cancer Res* 2001;61:5179–85.
- Motiwala T, Kutay H, Ghoshal K, et al. Protein tyrosine phosphatase receptor-type O (*PTPRO*) exhibits characteristics of a candidate tumor suppressor in human lung cancer. *Proc Natl Acad Sci U S A* 2004;101:13844–9.
- Trapasso F, Yendamuri S, Dumon KR, et al. Restoration of receptor-type protein tyrosine phosphatase η function inhibits human pancreatic carcinoma cell growth *in vitro* and *in vivo*. *Carcinogenesis* 2004;25:2107–14.
- Wang Z, Shen D, Parsons DW, et al. Mutational analysis of the tyrosine phosphatase in colorectal cancers. *Science* 2004;304:1164–6.